Optics Letters

High performance of a passively Q-switched mid-infrared laser with Bi_2Te_3/graphene composite SA

Zhenyu You,[1] Yijian Sun,[1,2] Dunlu Sun,[3] Zaojie Zhu,[1] Yan Wang,[1] Jianfu Li,[1] Chaoyang Tu,[1,6] and Jinlong Xu[4,5]

[1]Key Laboratory of Optoelectronic Materials Chemistry and Physics, Fujian Institute of Research on the Structure of Matter, Chinese Academy of Sciences, Fuzhou, Fujian 350002, China
[2]University of Chinese Academy of Sciences, Beijing 100039, China
[3]Key Laboratory of Photonic Devices and Materials, Anhui Province, Anhui Institute of Optics and Fine Mechanics, Chinese Academy of Sciences, Hefei 230031, China
[4]School of Electronic Science and Engineering, Nanjing University, Nanjing 210093, China
[5]e-mail: longno.2@163.com
[6]e-mail: tcy@fjirsm.ac.cn

Received 12 December 2016; revised 20 January 2017; accepted 23 January 2017; posted 25 January 2017 (Doc. ID 282346); published 14 February 2017

We report passively Q-switched ~2 and ~3 μm mid-infrared (MIR) solid-state lasers with a self-assembly solvothermal-synthesized Bi_2Te_3/graphene heterostructure saturable absorber (SA) for the first time. Based on the oxidation resistance and high thermal conductivity of graphene, and large modulation depth of Bi_2Te_3 nanosheets, two high-performance Q-switching lasers were realized. One is a Tm:YAP laser with a maximum average output power of 2.34 W and a pulse width of 238 ns at ~2 μm. The corresponding maximum pulse peak power was 91 W, which was much improved in comparison with the pure graphene-based Tm laser. The other one is an Er:YSGG laser producing a pulse width of 243 ns, which is the shortest among the 2D SAs-based ~3 μm solid-state lasers, as far as we know. Our results indicate that such a composite Bi_2Te_3/graphene material is a promising SA for generating high-performance mid-infrared pulse lasers.

OCIS codes: (140.3070) Infrared and far-infrared lasers; (160.4236) Nanomaterials; (140.3540) Lasers, Q-switched.

https://doi.org/10.1364/OL.42.000871

Due to their strong absorption in vapor, water, CO_2, and biological tissues, mid-infrared (MIR) lasers at ~2 and ~3 μm have attracted considerable attention for use in medical applications and laser radar measurements of atmospheric composition [1–3]. Compared to continuous-wave lasers, nanosecond solid-state MIR lasers show great advantages in accuracy because of their short pulses with high peak powers [4]. For these important practical applications, much effort has been given toward exploring high-performance MIR nanosecond lasers.

For pulsed lasers, passive Q-switching is a preferred method as a result of the simplicity, compactness, and low cost in design. In such lasers, saturable absorbers (SAs) are the key components, which absorb the low intensity light, and become transparent at high intensity. In the past decades, many kinds of SAs, including Cr:ZnSe, Co:ZnS, and semiconductor saturable absorber mirrors (SESAMs), have been used for passively Q-switched solid-state lasers [5–9]. However, in the MIR region, admirable SAs are still limited. Among these SAs, Fe:ZnSe etc., are wavelength-sensitive SAs in a given wavelength band [10,11]. SESAMs require complicated fabrication and packaging with high costs in general. Besides, suitable semiconductor materials for SESAMs in the mid-infrared region are also limited.

Graphene, a two-dimensional (2D) structure layered carbon material with Dirac-like gapless electronic band structure, has been widely investigated as an excellent optical SA from the visible to MIR wavelength bands. It reveals some advantages, including high optical nonlinear susceptibility, high carrier mobility, oxidation resistance, and high thermal conductivity, as well as the disadvantage of low modulation depth. Following graphene, some novel 2D nanomaterials, such as topological insulators (TIs) [12,13], transition metal disulfide (TMD) [14–16], and black phosphorus (BP) [17–20], have been verified to be SAs. Similar to graphene, TIs present a gapless metallic state in its edge/surface states, which results in a broadband saturable absorption. To date, TIs-based passively Q-switched solid-state lasers at 1.0, 1.3, and 1.5 μm have been successfully realized, respectively, while the laser performances in MIR wavelength bands reported are few. Furthermore, due to the easy oxidation at high temperature, and poor thermal conductivity, most of the pulse energies in the previous reports on TIs SAs were less than 4.0 μJ, and the pulse peak powers were limited under 3 W [21–24]. Such results will greatly limit their

applications. Thus, further investigation for high Q-switched laser performance is still very necessary.

In this Letter, we demonstrate passively Q-switched solid-state lasers at ~2 and ~3 μm MIR regions with a Bi_2Te_3/graphene (Bi_2Te_3/G) heterostructure SA for the first time. The Bi_2Te_3/G composites were fabricated by a facile self-assembly solvothermal route. Based on the oxidation resistance and high thermal conductivity of graphene, and large modulation depth of Bi_2Te_3 nanosheets, high-performance Q-switching operations in the MIR region were realized.

Because of the similar crystal structure and lattice parameters, Bi_2Te_3/G heterostructure can be efficiently fabricated by a facile self-assembly solvothermal route. In the previous reports, hexagonal Bi_2Te_3 nanosheets with uniform morphology were synthesized through a solvothermal route [25]. Keeping these conditions and adding additional graphene oxide (GO), the Bi_2Te_3 nucleus could be tightly adsorbed onto the GO surface and then be reduced by ethylene glycol (EG) to form Bi_2Te_3/G. In this process, the coverage of Bi_2Te_3 on graphene was tunable by controlling the mole ratio of Bi_2Te_3 and graphene oxide.

To analyze the structure and morphology of the Bi_2Te_3/G sample, a scanning electron microscope (SEM) and a transmission electron microscopy (TEM) were characterized and shown in Fig. 1. The SEM image reveals that uniform hexagonal Bi_2Te_3 nanosheets are grown on the surface of graphene, as shown in Fig. 1(a). Free Bi_2Te_3 nanosheets are seldom observed, even after a longtime ultrasonication. Resulting from the inhibition of graphene, the composite Bi_2Te_3 presents a smaller thickness in comparison with the pure one. From the TEM image in Fig. 1(b), the coverage of Bi_2Te_3 on graphene is estimated to be about 70%. The fine structure of the composites was also tested by HRTEM. As shown in Fig. 1(c), the lattice fringes of Bi_2Te_3 and graphene are clear, indicating the high quality of the composites. It can also be clarified by the selected area electron diffraction (SAED) where the bright diffraction spots belong to the Bi_2Te_3 crystal and the diffraction ring is of graphene. Figure 1(d) shows the linear transmission spectrum of Bi_2Te_3/G SA at the wavelength range of 1.9–3.0 μm measured using a FT-IR spectrometer (Lambda 950) that has excluded the influence of the substrate.

To clarify the nonlinear absorption characteristics of Bi_2Te_3/G SA in MIR regions, an open-aperture z-scan technology was employed. The Bi_2Te_3/G SA was prepared by a drop-coated method. The pump source used for z-scan measurement is a homemade optical parametric oscillator (OPO) laser with the emitting wavelength fixed at 2.8 μm and a pulse duration of 160 ns. The laser beam is focused to 50 μm at the focus position within the sample. As shown in Fig. 2(a), the z-scan normalized transmittance as a function of the sample position exhibits sharp and narrow peaks, which confirm the good nonlinear absorption characteristic of Bi_2Te_3/G SA. Figure 2(b) shows optical transmittances as increased excited intensity which is translated from the open-aperture z-scan curve. The corresponding data can be fitted by

$$T = 1 - \Delta R \cdot \exp(-I/I_s) - T_{ns}, \quad (1)$$

where ΔR is the modulation depth, T_{ns} is the nonsaturable loss, I is the exciting intensity, and I_s is the saturation intensity. The saturable trend of absorption could be obviously seen when the incident laser intensity increased. By fitting the curve, the modulation depth, saturation intensity, and nonsaturable loss were calculated to be 6.6%, 0.44 MW/cm^2, and 3.8%, respectively. Compared with the BP and WS_2 SAs in Refs. [26,27], the modulation depth of Bi_2Te_3/G SA is comparable, while the nonsaturable loss is relatively smaller. Such results will be beneficial for the high Q-switched laser performances in mid-infrared regions. Moreover, the modulation depth could be further increased with a thicker SA film.

The experimental setup is shown in Fig. 3. A compact plane-parallel cavity with a 10 mm length was used for the Bi_2Te_3/G SA-based Q-switched MIR lasers. Five millimeter long 5% Tm:YAP and 38% Er:YSGG were employed as the gain mediums for ~2 and 3 μm laser operations, respectively. The Tm:YAP crystal was cut along the a crystalline axis and Er:YSGG crystal in a random direction. Both of them were mounted into a water-cooled copper block cooled at 18°C. The pump sources were fiber-coupled LDs with a core diameter of 200 μm and a numerical aperture of 0.22. The emission wavelengths were 790 and 967 nm, respectively. The pump absorptions for Tm:YAP and Er:YSGG were 68% and 53%, respectively. IM was the input mirror, which was highly reflectively coated for the laser wavelength and antireflectively coated for the pump wavelength. The output coupling OC was coated with $T = 2\%$ transmission at the laser wavelength. To reduce the intracavity loss and improve the laser performance, the Bi_2Te_3/G composites were drop-coated on the OC mirror directly.

For the ~2 μm laser, it was of a CW laser operation mode with a pure OC mirror. When inserting the Bi_2Te_3/G SA-coated OC and increasing the absorbed pump power to 1.66 W, a stable passive Q-switching operation was achieved with an average output power of 87 mW. As shown in Fig. 4(a), the output power increased nearly linearly with the absorbed

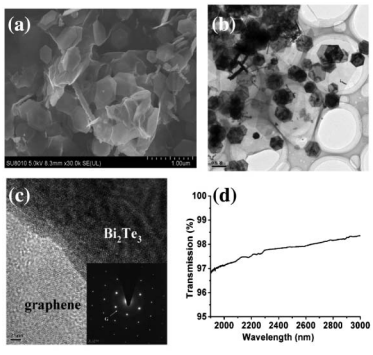

Fig. 1. Characterization of Bi_2Te_3/G sample: (a) SEM image, (b) TEM image, (c) lattice fringes of Bi_2Te_3 and graphene (inset is SAED image), and (d) transmission of Bi_2Te_3/G SA.

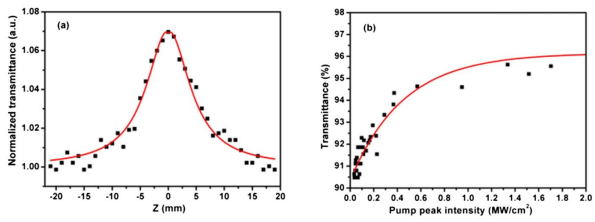

Fig. 2. (a) Z-scan curve and (b) nonlinear transmission as a function of pump peak intensity.

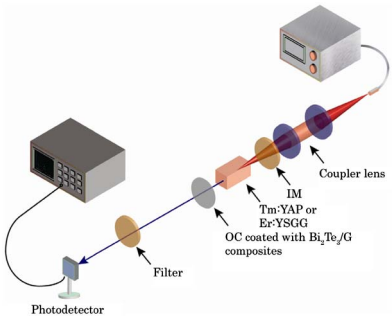

Fig. 3. Schematic setup of *Q*-switched Tm:YAP and Er:YSGG lasers with Bi_2Te_3/G SA.

pump power. At the absorbed pump power of 8.4 W, the highest average output power of 2.34 W with a slope efficiency of 32.3% and an optical-to-optical conversion of 27.9% were obtained. The wavelength of the laser was 1.98 μm with c-axis polarization. Figure 4(b) shows the pulse width and repetition rate as a function of absorbed pump power. Within the stable *Q*-switching regime, the pulse width and repetition rate varied from 1.22 μs to 238 ns and 46 kHz to 108 kHz, respectively. Under the maximum absorbed power, the highest pulse energy was 21.7 μJ, corresponding to the maximum pulse peak powers of 91 W. The typical *Q*-switched laser pulse trains and the single temporal pulse profile of the 238 ns pulse were shown in Fig. 5.

Table 1 summarizes the results ever obtained from ~2 μm passive *Q*-switching operations with other nano-SAs. It should be noted that, in addition to the SAs, cavity design may strongly influence the pulse duration. Due to the short round trip time with a microchip setup, the shortest pulses previously

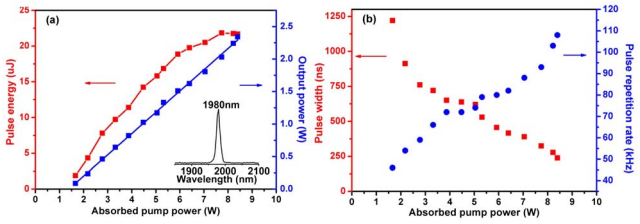

Fig. 4. (a) Single-pulse energy and output power. (b) Pulse width and repetition rate as a function of the absorbed pump power. The inset shows the spectrum of the laser.

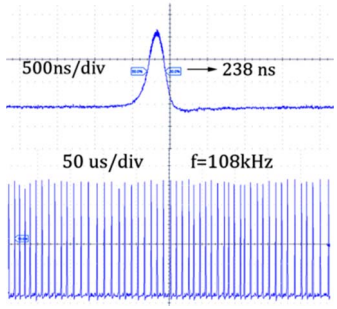

Fig. 5. Typical ~2 μm *Q*-switched pulse trains and the temporal pulse profile.

Table 1. Comparison of ~2 and ~3 μm Passively *Q*-Switched Laser Performance with Nano-SAs (Upper Part for 2 μm and Lower Part for 3 μm)

SA	Gain Medium	Output Power (mW)	Pulse Width (ns)	Peak Power (W)	Ref.
Bi_2Te_3/G	Tm:YAP	2340	238	91	This work
BP	Tm:YAG	38.5	3120	1.1	[18]
BP	Tm:YAP	3100	181	218	[20]
WS_2	Tm:LuAG	1080	660	26	[27]
SWCNTs	Tm:KLuW	700	25	45	[28]
Graphene	Ho:YAG	640	170	21	[29]
Graphene	Tm:LGGG	2260	1290	2.47	[30]
Graphene	Ho:YVO_4	2200	265	63.3	[31]
Graphene	Tm:YAP	362	735	11.6	[32]
Gold nanorods	Tm:YAG	380	796	6.2	[33]
MoS_2	Tm:Ho:YGG	206	410	3.4	[15]
MoS_2	Tm:CLNGG	62	4840	0.15	[34]
MoS_2	Tm:$GdVO_4$	100	800	2.6	[35]
Bi_2Te_3/G	Er:YSGG	110	243	5.14	This work
MoS_2	Er:Lu_2O_3	1030	335	23.8	[14]
BP	Er:Y_2O_3	6	4470	0.11	[26]
Graphene	Er:CaF_2	172	1324	2.07	[36]

achieved at 2 μm with single-walled carbon nanotubes (SWCNTs) were in the order of 25 ns [28]. A 170 ns pulse width of a graphene *Q*-switched Ho:YAG microchip laser was achieved as well for the same reason [29]. Our results can be considered superior to the results by utilizing WS_2, MoS_2, graphene, and gold nanorod SAs. In comparison with other results, although the BP *Q*-switched Tm:YAP laser in Ref. [20] has a bit shorter pulses and higher peak power, the shortcoming of instability in air limits the application of BP in generating short pulse lasers in many situations. We believe that better performance can be realized by further optimizing the parameters of the cavity (such as cavity structure and transmission of OC) and the SA film (such as the thickness of the film and the coverage of Bi_2Te_3/G).

For the ~3 μm laser, stable passively *Q*-switched pulses were also realized. The temporal traces of *Q*-switched pulse trains are shown in Fig. 6(a). At an output power of 110 mW, a narrowest pulse width of 243 ns was obtained with a repetition rate of 88 kHz. The maximum peak power was estimated to be 5.14 W, corresponding to the highest pulse energy of 1.25 μJ. The center wavelength of the laser was located at

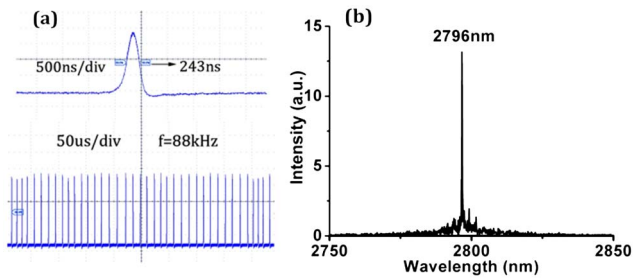

Fig. 6. (a) A typical ~3 μm *Q*-switched pulse train and temporal pulse profile. (b) Output spectrum of passively *Q*-switched Er:YSGG laser.

2796 nm, as shown in Fig. 6(b). Note that stable Q-switching only could be achieved in a narrow power range (~20 mW), beyond where unstable Q-switched pulses were observed. We think the possible reason contributing to the result is as follows. Because of the high doping concentration in the laser crystal, the Er^{3+} ions have abundant energy transfer processes. These processes, including cross-relaxation, upconversion and reabsorption, will result in an unstable population in the upper level $^4I_{11/2}$ and lower level $^4I_{13/2}$, especially when the pumping power is enhanced. In this case, the parameters of the laser cavity and SA film should be more optimized for achieving stable pulses. Despite this, as far as we know, the pulse width achieved in this work is the shortest among Q-switched ~3 μm Er lasers based on 2D-SA, as shown in Table 1.

Nano-SAs and SESAMs, both being fast SAs, and Bi_2Te_3/G SAs show some advantages due to their broadband saturable absorption. Though a shorter pulse width may be achieved with SESAMs, most of the SESAMs are wavelength-sensitive and respond to light at a given wavelength band. Nonetheless, the Bi_2Te_3/G SA can be applied in a wide range of wavelength regions. Meanwhile, the fabrication process of nano-SAs is simple and the cost is low relative to SESAMs.

In conclusion, a Bi_2Te_3/G heterostructure was prepared by a facile self-assembly solvothermal technique and its nonlinear saturable absorption properties were investigated. Passively Q-switched Tm:YAP and Er:YSGG lasers at ~2 and ~3 μm, respectively, were demonstrated by utilizing the Bi_2Te_3/G SA for the first time. At the ~2 μm waveband, the maximum output power was 2.34 W at an absorbed pump power of 8.4 W, corresponding to a pulse width of 238 ns and a repetition rate of 108 kHz, resulting in a pulse energy of 21.7 μJ and a peak power of 91 W. Moreover, an average output power of 110 W with a narrowest pulse width of 243 ns and a repetition rate of 88 kHz were obtained at ~3 μm, with the corresponding highest pulse energy and peak power of 1.25 μJ and 5.14 W, respectively. The experimental results definitely demonstrate that Bi_2Te_3/G SA is a class of high-performance broadband SA for MIR Q-switched lasers.

Funding. National Natural Science Foundation of China (NSFC) (11304313, 51472240, 61675204); National Key Research and Development Program of China (2016YFB0701002); Strategic Priority Research Program of the Chinese Academy of Sciences (CAS) (XDB20010200); Nature Science Foundation of Fujian Province (2015I0007, 2015J05134).

REFERENCES

1. H. A. Wigdor, J. T. Walsh, Jr., J. D. B. Featherstone, S. R. Visuri, D. Fried, and J. L. Waldvogel, Lasers Surg. Med. **16**, 103 (1995).
2. Q. Ren, V. Venugopalan, K. Schomacker, T. F. Deutsch, T. J. Flotte, C. A. Puliafito, and R. Birngruber, Lasers Surg. Med. **12**, 274 (1992).
3. L. I. Deckelbaum, Lasers Surg. Med. **15**, 315 (1994).
4. S. T. Hendow and S. A. Shakir, Opt. Express **18**, 10188 (2010).
5. A. Aubourg, J. Didierjean, N. Aubry, F. Balembois, and P. Georges, Opt. Lett. **38**, 938 (2013).
6. T. Tsai and M. Birnbaum, J. Appl. Phys. **89**, 2006 (2001).
7. B. Q. Yao, Y. Tian, G. Li, and Y. Z. Wang, Opt. Express **18**, 13574 (2010).
8. M. Segura, M. Kadankov, X. Mateos, M. C. Pujol, J. J. Carvajal, M. Aguiló, F. Díaz, U. Griebner, and V. Petrov, Opt. Express **20**, 3394 (2012).
9. Z. S. Qu, Y. G. Wang, J. Liu, L. H. Zheng, L. B. Su, and J. Xu, Appl. Phys. B **109**, 143 (2012).
10. A. A. Voronov, V. I. Kozlovskii, Y. V. Korostelin, A. I. Landman, Y. P. Podmar'kov, V. G. Polushkin, and M. P. Frolov, Quantum Electron. **36**, 1 (2006).
11. A. Martinez, A. R. Gallian, P. Marine, V. Fedorov, S. Mirov, and V. Badikov, *Advanced Solid-State Photonics*, OSA Technical Digest (Optical Society of America, 2007), paper TuB24.
12. C. J. Zhao, H. Zhang, X. Qi, Y. Chen, Z. T. Wang, S. C. Wen, and D. Y. Tang, Appl. Phys. Lett. **101**, 211106 (2012).
13. J. F. Li, H. Y. Luo, L. L. Wang, C. J. Zhao, H. Zhang, H. P. Li, and Y. Liu, Opt. Lett. **40**, 3659 (2015).
14. M. Q. Fan, T. Li, S. Z. Zhao, G. Q. Li, H. Y. Ma, X. C. Gao, C. Kränkel, and G. Huber, Opt. Lett. **41**, 540 (2016).
15. S. X. Wang, H. H. Yu, H. Zhang, A. Z. Wang, M. W. Zhao, Y. X. Chen, L. M. Wei, and J. Y. Wang, Adv. Mater. **26**, 3538 (2014).
16. Z. Tian, K. Wu, L. C. Kong, N. Yang, Y. Wang, R. Chen, W. S. Hu, J. Q. Xu, and Y. L. Tang, Laser Phys. Lett. **12**, 065104 (2015).
17. S. B. Lu, L. L. Miao, Z. N. Guo, X. Qi, C. J. Zhao, H. Zhang, S. C. Wen, D. Y. Tang, and D. Y. Fan, Opt. Express **23**, 11183 (2015).
18. Y. X. Xie, L. C. Kong, Z. P. Qin, G. Q. Xie, and J. Zhang, Opt. Eng. **55**, 081307 (2016).
19. H. Yu, X. Zheng, K. Yin, X. A. Cheng, and T. Jiang, Opt. Mater. Express **6**, 603 (2016).
20. H. K. Zhang, J. L. He, Z. W. Wang, J. Hou, B. T. Zhang, R. W. Zhao, K. Z. Han, K. J. Yang, H. K. Nie, and X. L. Sun, Opt. Mater. Express **6**, 2328 (2016).
21. Y. J. Sun, C. K. Lee, J. L. Xu, Z. J. Zhu, Y. Q. Wang, S. F. Gao, H. P. Xia, Z. Y. You, and C. Y. Tu, Photon. Res. **3**, A97 (2015).
22. J. L. Xu, Y. J. Sun, J. L. He, Y. Wang, Z. J. Zhu, Z. Y. You, J. F. Li, M. C. Chou, C. K. Lee, and C. Y. Tu, Sci. Rep. **5**, 14856 (2015).
23. B. L. Wang, H. H. Yu, H. Zhang, C. J. Zhao, S. C. Wen, H. J. Zhang, and J. Y. Wang, IEEE Photon. J. **6**, 1501007 (2014).
24. H. H. Yu, H. Zhang, Y. C. Wang, C. J. Zhao, B. L. Wang, S. C. Wen, H. J. Zhang, and J. Y. Wang, Laser Photon. Rev. **7**, L77 (2013).
25. Y. Zhang, L. P. Hu, T. J. Zhu, J. Xie, and X. B. Zhao, Cryst. Growth Des. **13**, 645 (2013).
26. L. C. Kong, Z. P. Qin, G. Q. Xie, Z. N. Guo, H. Zhang, P. Yuan, and L. J. Qian, Laser Phys. Lett. **13**, 045801 (2016).
27. C. Luan, K. J. Yang, J. Zhao, S. J. Zhao, L. Song, T. Li, H. W. Chu, J. P. Qiao, C. Wang, Z. Li, S. Z. Jiang, B. Y. Man, and L. H. Zheng, Opt. Lett. **41**, 3783 (2016).
28. P. Loiko, X. Mateos, S. Y. Choi, F. Rotermund, J. M. Serres, M. Aguiló, F. Díaz, K. Yumashev, U. Griebner, and V. Petrov, J. Opt. Soc. Am. B **33**, D19 (2016).
29. R. Lan, P. Loiko, X. Mateos, Y. Wang, J. Li, Y. Pan, S. Y. Choi, M. H. Kim, F. Rotermund, A. Yasukevich, K. Yumashev, U. Griebner, and V. Petrov, Appl. Opt. **55**, 4877 (2016).
30. J. Hou, Z. T. Jia, B. T. Zhang, Y. R. Yin, J. Ning, W. X. Mu, K. Z. Han, J. L. He, and X. T. Tao, IEEE Photon. Technol. Lett. **28**, 825 (2016).
31. W. M. Lin, X. M. Duan, Z. Cui, B. Q. Yao, T. Y. Dai, and X. L. Li, Appl. Sci. **6**, 128 (2016).
32. J. Hou, B. T. Zhang, J. L. He, Z. W. Wang, F. Lou, J. Ning, R. W. Zhao, and X. C. Su, Appl. Opt. **53**, 4968 (2014).
33. H. T. Huang, M. Li, P. Liu, L. Jin, H. Wang, and D. Y. Shen, Opt. Lett. **41**, 2700 (2016).
34. L. C. Kong, G. Q. Xie, P. Yuan, L. J. Qian, S. X. Wang, H. H. Yu, and H. J. Zhang, Photon. Res. **3**, A47 (2015).
35. P. G. Ge, J. Liu, S. Z. Jiang, Y. Y. Xu, and B. Y. Man, Photon. Res. **3**, 256 (2015).
36. C. Li, J. Liu, S. Z. Jiang, S. C. Xu, W. W. Ma, J. Y. Wang, X. D. Xu, and L. B. Su, Opt. Mater. Express **6**, 1570 (2016).